

Measurement report: Crustal materials play an increasing role in elevating particle pH: Insights from 12-year records in a typical inland city of China.

Hongyu Zhang^{1,2}, Shenbo Wang^{2,3*}, Zhangsen Dong^{1,2*}, Xiao Li^{2,3}, Ruiqin Zhang^{2,3}

¹ Collage of Chemistry, Zhengzhou University, Zhengzhou, 450000, China

² Research Institute of Environmental Sciences, Zhengzhou University, Zhengzhou 450000, China

³ School of Ecology and Environment, Zhengzhou University, Zhengzhou, 450000, China

* Corresponding authors: Shenbo Wang and Zhangsen Dong

E-mail address: shbwang@zzu.edu.cn and dzszzu1990@163.com

14 **Abstract**

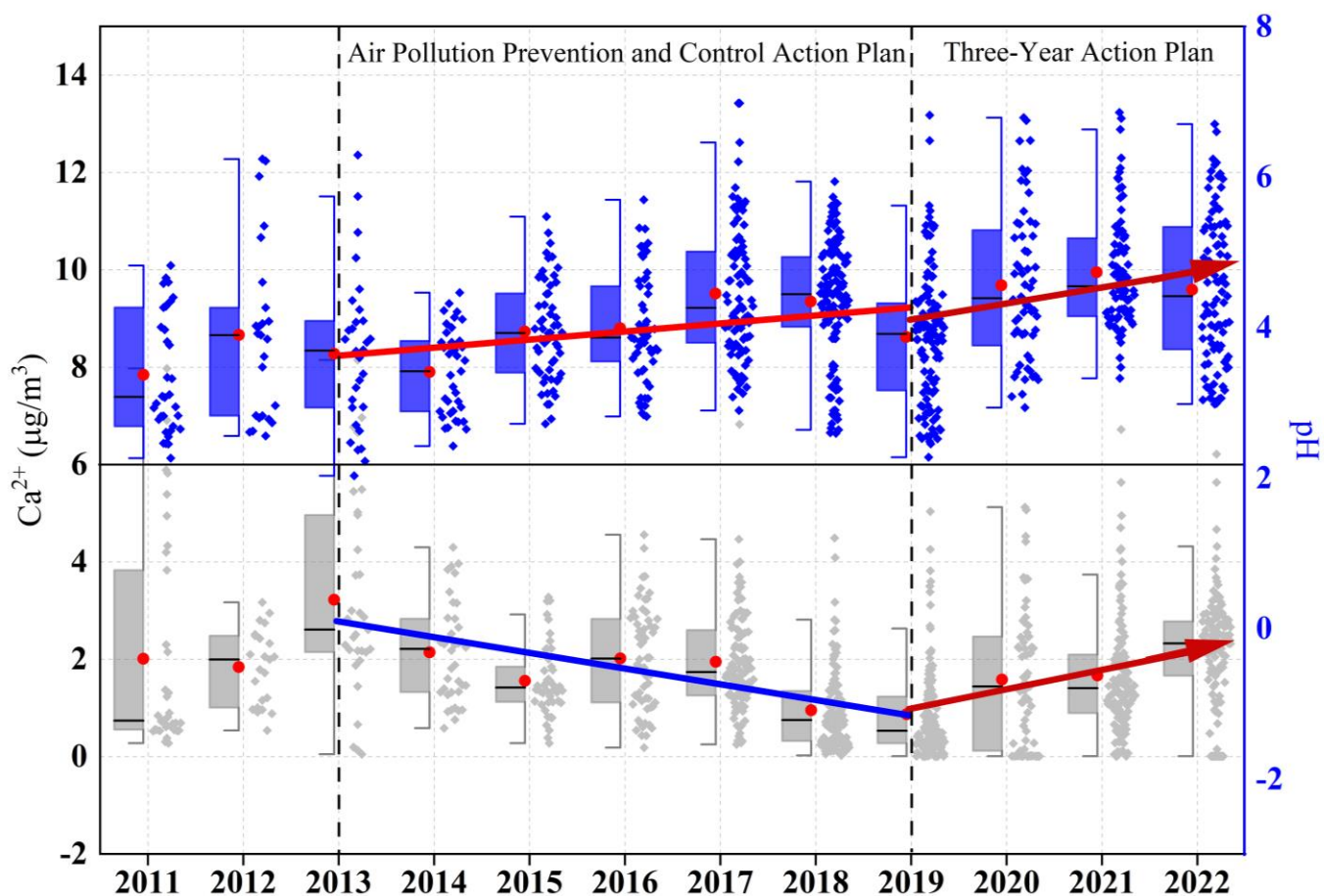
15 Particle acidity serves as a key determinant in atmospheric chemical processes. Emerging concerns
16 regarding aerosol acidity trends have been highlighted amid China's sustained initiatives to mitigate
17 emissions of both acidic and alkaline precursors, especially in North China, which is significantly
18 affected by dust aerosol. 12-year observational data in Zhengzhou reveal that the annual average PM_{2.5}
19 concentration decreased from $162 \pm 81 \text{ } \mu\text{g}/\text{m}^3$ in 2011 to $60 \pm 41 \text{ } \mu\text{g}/\text{m}^3$ in 2022, with the largest
20 reduction in sulfate (73%). Correspondingly, the annual particle pH increased by 0.10 units from 2011
21 to 2019. In addition, the elevated particle pH in 2015 and 2018 was notably influenced by the increase
22 in TNH_x (NH₃ + NH₄⁺). Note that the crustal material concentrations and their proportions increased
23 significantly during 2019–2022, which might be responsible for the resuspension of surrounding soil
24 dust. Even though the TNH_x concentration was decreasing, the annual average growth rate of pH
25 values increased to 0.21 units from 2019 to 2022. This phenomenon is not unique to Zhengzhou, as
26 major cities in the North China Plain have also experienced a pronounced upward trend in coarse
27 particles after 2019. Therefore, the long-term evolution of particle acidity in North China will require
28 comprehensive consideration of synergistic effects involving acidic precursors, ammonia, and crustal
29 materials.

30 **Keywords:** Dust, aerosol acidity, sources, North China Plain, control measurement

31

32 **Synopsis:** The future ammonia reduction policies in North China may not lead to a rapid increase in
33 particle acidity in the presence of crustal materials., which further elevated the particle pH after 2019.

34 **Graphical abstract:**



35

36

37

38 **Highlights:**

- 39 • Crustal material concentrations and their proportions increased significantly during 2019–2022;
- 40 • The resuspension of surrounding soil dust may determine the rebound of crustal material
- 41 concentrations;
- 42 • Rebound in crustal material further elevated the particle pH.

43

44 **1 Introduction**

45 Particle acidity is a critical parameter that affects atmospheric chemistry, such as the gas-particle
46 partitioning of semi-volatile and volatile species (Surratt et al., 2010; Guo et al., 2016), the solubility
47 of metals (Tao and Murphy, 2019), acid-catalyzed reactions (Rengarajan et al., 2011), and acid
48 deposition (Mao et al., 2009), thereby determining aerosol concentration and chemical composition,
49 as well as impacting human health, ecosystems, and climate (Li et al., 2017; Pye et al., 2020; Su et al.,
50 2020; Nenes et al., 2021). Generally, the global fine particulate matter (PM_{2.5}, aerodynamic diameter
51 $\leq 2.5 \mu\text{m}$) exhibits a bimodal pH distribution ranging from 1–3 (e.g., in the United States and Europe)
52 (Guo et al., 2015; Battaglia et al., 2017; Masiol et al., 2020; Zhang et al., 2021) and 4–5 (e.g., in East
53 Asia) (Kim et al., 2022; Sharma et al., 2022). The atmosphere rich in gaseous ammonia (NH₃) and
54 crustal material (CM) shows significant pH buffering effects (Wang et al., 2020; Zheng et al., 2020;
55 Karydis et al., 2021), which is a dominant factor that drives the high particle pH in East Asia (Karydis
56 et al., 2021; Zhang et al., 2021; Kim et al., 2022; Sharma et al., 2022).

57 In recent years, the changing trends in particle pH have become a research focus, especially in
58 China, in response to air pollution control policies, i.e. Air Pollution Prevention and Control Action
59 Plan (2013–2018) and Three-Year Action Plan (2018–2020). The annual average PM_{2.5} concentration
60 in Beijing dropped by 64% from 89.5 $\mu\text{g}/\text{m}^3$ in 2013 to 32 $\mu\text{g}/\text{m}^3$ in 2023 (MEP, 2023), with a clear
61 downward trend of sulfate concentration, and nitrate surpassing sulfate as the primary component
62 (Zhai et al., 2019; Zhou et al., 2019; Li et al., 2023). The atmospheric behavior of ammonium, governed
63 by gas-particle partitioning processes involving ammonia (NH₃) as the predominant alkaline gas,

64 demonstrates notable stability in concentration levels, with observational records showing less than 5%
65 interannual variation in NH_3 column densities over North China during 2015–2019 (Dong et al., 2023).
66 Under such conditions, the dominant inorganic aerosol component transitions from ammonium sulfate
67 to ammonium nitrate. This compositional shift enhances atmospheric particulate hygroscopicity due
68 to ammonium nitrate's superior water uptake capability, ultimately elevating particle pH levels through
69 aqueous-phase dilution mechanisms (Wexler and Seinfeld, 1991; Pinder et al., 2007, 2008; Heald et
70 al., 2012; Weber et al., 2016). For instance, a significant increase in the nitrate-to-sulfate molar ratio
71 from 2014–2017 in Beijing resulted in the particle pH increasing from 4.4 to 5.4 (Xie et al., 2020).
72 Moreover, increased NH_3 concentrations raised particle pH by 0.3–0.4 units from 2014/2015 to
73 2018/2019 in Beijing (Song et al., 2019). Over Europe and North America, the pH has increased
74 strongly from about 2.8 and 2.2 during the 1970s to 3.9 and 3.3 in 2020 respectively, especially during
75 the 1990s, with significantly increasing NH_3 emission (Karydis et al., 2021). On the contrary, modeling
76 results indicate a continuous decline in pH in East Asia from 1970 to 2020 due to sharp increases in
77 SO_2 and NO_x emissions (Karydis et al., 2021). In addition, the $\text{PM}_{2.5}$ pH showed a slight decrease of
78 0.13 from 2018 to 2022 summer in Beijing due to the change in total nitrate ($\text{NO}_3^- + \text{HNO}_3$) (Li et al.,
79 2023). Moreover, Zhou et al. (2022) found a decreasing pH trend from 2011 to 2019 in eastern China,
80 primarily influenced by temperature, followed by sulfate and non-volatile cations. Similarly, Nah et al.
81 (2023) observed a decreasing pH trend from 2011 to 2020 in Hong Kong, attributing it to temperature
82 and sulfate levels. Thus, concerns have been raised about the potential increase in the acidity of aerosol
83 and precipitation due to China's ongoing efforts to reduce ammonia emissions, which pose severe
84 health risks and acid deposition (Liu et al., 2019; Shi et al., 2019).

In addition to NH_3 , CM is another key alkaline substance that buffers particle pH. Ca^{2+} can form insoluble CaSO_4 with sulfate, reducing sulfate concentration in the aqueous phase of aerosol, and thus lowering H^+ and aerosol liquid water content (ALWC) concentrations and enhancing particle pH (Ding et al., 2019; Karydis et al., 2021). Moreover, non-volatile cations can lower the molar ratio of ammonia to sulfate, leading to an increase in particle pH (Zheng et al., 2022). Karydis et al. (2021) framework demonstrated that CM played a critical buffering role in sustaining aerosol pH around 7 across the Middle East arid regions. The model sensitivity tests revealed that under hypothetical dust-free conditions ($\text{CM} = 0$), aerosol acidity would escalate to $\text{pH} \sim 4$ due to $\text{NH}_4^+ / \text{SO}_4^{2-}$ domination. Wang et al. (2022) reported that non-volatile cations accounted for approximately 8–17% of hourly aerosol pH variation. Li et al. (2023) indicated that the buffering effect of cations was the major reason for the relatively small pH changes from 2018 to 2022 in Beijing, emphasizing that reducing coarse particle emissions in the future could significantly decrease particle pH. In addition, there was a rising trend in the contribution of CM to particle pH in Tianjin, China (Shi et al., 2017). Therefore, it is evident that CM has a significant impact on the variation of particle pH, especially in North China, which is significantly affected by dust aerosol, but the trend of CM concentration and its long-term implications is still lacking unfortunately.

Zhengzhou presents unique atmospheric chemistry that distinguishes it from other mega-cities in North China. As the capital of China's foremost agricultural province (Henan Province, contributing 18% of national NH_3 emissions), Zhengzhou's $\text{PM}_{2.5}$ composition combined substantial crustal material ($15 \pm 3\%$ in $\text{PM}_{2.5}$ vs. $<10\%$ in Beijing) with exceptional ammonia abundance (Huang et al., 2012; Liu et al., 2018; Wang et al., 2018). This created distinct particle acidity characteristics,

maintaining pH 4.5–6.0 compared to lower pH levels (3.3–5.4) in other cities like Beijing (Ding et al., 2019; Zhang et al., 2021). However, two critical research gaps persist: (1) the long-term evolution of CM under control policies remains unquantified; (2) the role of CM on pH buffer capacity in NH₃-enriched environments lacks systematic assessment.

To address these gaps, our study pioneers the first multi-decadal analysis (2011–2022) coupling PM_{2.5} components with thermodynamic modeling through three key innovations: (1) revealing the long-term trends of CM, (2) analyzing the variations of CM sources, and (3) exploring pH trend and its relationship with CM. The resultant findings advance our understanding of urban aerosol acidity chemistry by underscoring the critical role of CM.

2 Experiment and method

2.1 Instruments and Measurements

Sampling was conducted on the fourth-floor platform at Zhengzhou University (34.75° N, 113.61° E) in Zhengzhou, China. The sampling site (Fig. S1), approximately 14 m above the ground, is primarily surrounded by residential areas with well-developed transportation networks and no significant industrial sources. There are two highways located 3 km to the south and 7 km to the east. Additionally, a coal-fired power plant located 6 km to the east was shut down in 2020, and a gas-fired power plant is situated 3 km to the south.

Samples were collected using a high-volume sampler (TE-6070D, Tisch, USA) and air particulate samplers (TH-16A, Tianhong, China) from April 2011 to December 2022. Two quartz filters and two

125 Teflon filters were used daily from 10:00 AM to 9:00 AM the next day, resulting in a total of 5848
126 samples. After excluding abnormal data due to instrument malfunctions, 4228 valid samples were
127 obtained. Detailed information on the samples is provided in Table S1. Organic carbon (OC) and
128 elemental carbon (EC) were analyzed using a carbon analyzer (Model 5L, Sunset Laboratory, USA).
129 Water-soluble inorganic ions (Cl^- , NO_3^- , SO_4^{2-} , Na^+ , NH_4^+ , K^+ , Mg^{2+} , and Ca^{2+}) were measured using
130 ion chromatography (ICS-90 and ICS-900 models, Dionex, USA) (Yu et al., 2017; Jiang et al., 2018).
131 Elements were analyzed using a wavelength dispersive X-ray fluorescence spectrometer (S8 TIGER,
132 Bruker, Germany) to determine concentrations of Fe, Na, Mg, Al, Si, Cl, K, Ca, V, Ni, Cu, Zn, Cr, Mn,
133 Co, Cd, Ga, As, Se, Sr, Sn, Sb, Ba, and Pb (Tremper et al., 2018). Meteorological conditions, including
134 temperature (T), relative humidity (RH), and wind speed (WS) were obtained using an automatic
135 weather station (Wang et al., 2019). Blank filters were also routinely analyzed with each batch of
136 samples to detect sample contamination and provide quality assurance on the elemental concentrations.
137 Detailed analytical methods and quality control are described in the supplement (Text S1). The method
138 detection limits and measurement uncertainties are summarized in Table S2. The quality assurance
139 protocol excluded temporally discrete dust storm and precipitation periods to prevent contamination
140 of the source analysis of CM and modeling particle pH, given that such events induce non-
141 representative extremes in both crustal element concentrations and pH values, coupled with elevated
142 PM measurement uncertainties. The annual mean $\text{PM}_{2.5}$ concentration data for cities in the North China
143 Plain were obtained from the China National Environmental Monitoring Center (CNEMC), available
144 at <https://www.cnemc.cn/>.

2.2 Data Analysis

2.2.1 Mass reconstruction

The calculation method for CM is as follows (Tian et al., 2016):

$$[CM] = 1.89 \times [Al] + 2.14 \times [Si] + 1.4 \times [Ca] + 1.43 \times [Fe] + 1.94 [Ti] \quad (1)$$

where [Al], [Si], [Ca], [Fe] and [Ti] represent the concentrations of the respective elements ($\mu\text{g}/\text{m}^3$), but Ti was not measured.

2.2.2 Thermodynamic model

The particle pH was calculated using the ISORROPIA-II mode (version 2.1, <http://isorropia.eas.gatech.edu>). The input data (excluding $RH \leq 30\%$), including SO_4^{2-} , TNO_3 ($\text{HNO}_3 + \text{NO}_3^-$), TNH_x ($\text{NH}_3 + \text{NH}_4^+$), Ca^{2+} , K^+ , Na^+ , Mg^{2+} , Cl^- , RH and T , with the temporal resolution aligned with the sampling periods (from 10:00 AM to 9:00 AM the following day). The concentrations of hydrogen ions in air (H_{air}^+) and $ALWC$ were derived from the $\text{Na}^+ - \text{K}^+ - \text{Ca}^{2+} - \text{Mg}^{2+} - \text{NH}_4^+ - \text{SO}_4^{2-} - \text{NO}_3^- - \text{Cl}^- - \text{H}_2\text{O}$ equilibrium composition system. Activity coefficients for H^+ and OH^- were fixed at unity, while other ion pairs (e.g., $\text{H}^+ - \text{Cl}^-$) employed the Kusik-Meissner parameterization for ionic activity calculations (Fountoukis and Nenes, 2007). pH values were calculated using the following formula:

$$\text{pH} = -\log_{10} \text{H}_{\text{aq}}^+ \cong -\log_{10} \frac{1000 \text{H}_{\text{air}}^+}{ALWC_i + ALWC_o} \cong -\log_{10} \frac{1000 \text{H}_{\text{air}}^+}{ALWC_i} \quad (2)$$

$$ALWC_o = \frac{m_{org} \rho_w}{\rho_w} \frac{\kappa_{org}}{\left(\frac{1}{RH} - 1 \right)} \quad (3)$$

where $ALWC_i$ and $ALWC_o$ refer to the $ALWC$ for inorganic and organic components, respectively.

163 m_{org} denotes the mass of organic aerosol, ρ_w is the density of water (1.0 g/cm³), ρ_{org} is the density of
 164 organic material (1.4 g/cm³) (Guo et al., 2015), k_{org} is the hygroscopicity parameter for organic aerosol
 165 (0.087) (Chang et al., 2010; Li et al., 2016). The ISORROPIA-II model operated under metastable
 166 conditions in the forward mode. Due to the lack of measured data for gaseous HNO₃ and NH₃, TNO₃
 167 was represented solely by NO₃⁻. The concentration of NH₃ was simulated based on a linear regression
 168 equation proposed by Wei et al. (2023), who used the same data as this study from 2013 to 2020:

$$169 \quad \text{NH}_3 = 19.909 \times \text{RH} + 0.559 \times \text{T} - 0.35 \times \text{NH}_4^+ + 0.123 \times \text{NO}_3^- + 2.159 \times \text{Cl}^- - 0.224 \times \text{SO}_4^{2-} - 154.923 \quad (4)$$

170 where NO₃⁻, SO₄²⁻, NH₄⁺, and Cl⁻ correspond to their respective concentrations (μg/m³). To validate
 171 the applicability of Equation 4 for annual NH₃ estimation and pH simulation in Zhengzhou, this study
 172 utilized both observed NH₃ data (from a Thermo Scientific URG-9000D ambient ion monitor, USA)
 173 and calculated NH₃ values derived from Equation 4 at the same monitoring site throughout 2022,
 174 inputting them into the thermodynamic model for pH simulation. As shown in Figure S2, pH values
 175 calculated from observed and simulated NH₃ exhibit good agreement ($r = 0.97$, $P < 0.01$). Furthermore,
 176 NH₃ concentrations modeled by ISORROPIA demonstrate a significant correlation ($r = 0.95$, $P < 0.01$)
 177 with that simulated NH₃ by Equation 4. These results collectively demonstrate the reliability of the
 178 NH₃ estimation method in this study.

179 **2.2.3 HYSPLIT analysis**

180 Backward trajectories were calculated using the mixed-particle Lagrangian integrated trajectory
 181 method (HYSPLIT, [https:// www.ready.noaa.gov/HYSPLIT_traj.php](https://www.ready.noaa.gov/HYSPLIT_traj.php)). Meteorological input data were
 182 from the Global Data Assimilation System (GDAS) with 3D wind vectors, temperature, relative

183 humidity, geopotential height, surface pressure, and boundary layer diagnostics. 24-hour backward
184 trajectories were simulated for air masses arriving at 100 m above ground level in Zhengzhou, a
185 receptor height aligned with the city's average elevation (~100 m above sea level) to capture near-
186 surface pollutant transport dynamics within the boundary layer.

187 Trajectories from 2013–2018 and 2019–2022 were independently clustered via the Angle Distance
188 algorithm to compare policy-driven variations (Wang et al., 2009). The optimal cluster number (three,
189 Figure S3) was determined by tracking total spatial variance (TSV), with classification finalized at the
190 inflection point preceding the second TSV surge.

191 **3 Results and discussion**

192 **3.1 Temporal variations in chemical components**

193 Over the past twelve years, the Chinese government has implemented two major policies to
194 mitigate air pollution: the Air Pollution Prevention and Control Action Plans (2013–2018) and the
195 Three-Year Action Plan (2018–2020), with key targets and measures detailed in Tables S3 and S4. The
196 2013–2018 policy prioritized end-of-pipe controls in power generation and heavy industries,
197 mandating $\geq 10\%$ PM₁₀ reduction nationwide and region-specific PM_{2.5} reduction targets (25% for
198 Beijing-Tianjin-Hebei, 20% for Yangtze River Delta, and 15% for Pearl River Delta). Subsequently,
199 the 2018–2020 campaign shifted toward structural reforms and multi-pollutant synergistic governance,
200 enforcing $\geq 15\%$ nationwide SO₂/NO_x emission cuts and $\geq 18\%$ PM_{2.5} reduction in non-compliant cities
201 relative to 2015 levels.

The long-term trends in PM_{2.5} concentrations and its chemical components in Zhengzhou from 2011 to 2022 are depicted in Fig. 1, with annual average concentrations listed in Table 1. Correspondingly, the annual average concentration of PM_{2.5} in Zhengzhou decreased from 162 ± 81 µg/m³ in 2011 to 60 ± 41 µg/m³ in 2022, representing a reduction of approximately 63%. In particular, the reduction rate reached 72% after 2013. As for chemical components, the largest reductions were observed in SO₄²⁻ (79%), decreasing from 38.0 ± 19.9 µg/m³ in 2013 to 7.9 ± 4.5 µg/m³ in 2022, followed by EC (76%). Additionally, the concentrations of NH₄⁺ and NO₃⁻ also significantly decreased by 68% and 56%, respectively. The proportion of each component in PM_{2.5} (Fig. S4) reveals a decrease in SO₄²⁻, K⁺, and Cl⁻, indicating effective control measures targeting coal and biomass combustion (Lei et al., 2021). However, the proportions of NO₃⁻ and OC in PM_{2.5} rose from 11% and 12% in 2013 to 13% and 17% in 2022, respectively, similar to the trend observed in the North China Plain (Wen et al., 2018; Zhai et al., 2019; Li et al., 2023).

3.2 Temporal variations in CM

Notably, there is no clear declining trend in the CM concentration, with a rebound observed during 2020–2022 (Fig. 1i). Furthermore, the proportion of CM in PM_{2.5} exhibits a significant upward trend (Fig. S4). To further analyze its trend, sampling data were divided into three periods corresponding to governmental stages: 2011–2013, when no special control measures were implemented; 2013–2019, coinciding with the implementation of the Air Pollution Prevention and Control Action Plan; and 2019–2022, coinciding with the Three-Year Action Plan. During these periods, Henan Province and Zhengzhou City implemented several dust control policies summarized in Table S5. As shown in Fig.

222 2a and 2b, the mass concentration of CM peaked at $14.6 \pm 8.3 \mu\text{g}/\text{m}^3$ in 2013, accounting for 8% of
 223 $\text{PM}_{2.5}$. To evaluate the inter - annual change trend of CM, the Mann - Kendall method, Sen's slope,
 224 and Least - Squares (LS) slope were comprehensively used with the results presented in Table S6.
 225 From 2013 to 2019, the CM concentration notably decreased from 14.6 ± 8.3 to $8.5 \pm 7.8 \mu\text{g}/\text{m}^3$, with
 226 an annual average decline rate of $0.81 \mu\text{g}/(\text{m}^3 \cdot \text{year})$ from LS slope [$0.015 \mu\text{g}/(\text{m}^3 \cdot \text{year})$ from Sen's
 227 slope]. Apart from control measures, the interannual meteorological analysis shows (Fig. S5) WS
 228 exhibited a declining trend, with a decrease rate of 43%, while RH showed an increasing trend at a rate
 229 of 8% from 2013 to 2019, under which conditions that were unfavorable for dust resuspension (Wang
 230 et al., 2013, 2018). Seasonal trends (Fig. S6) reveal significant declines in CM during spring in 2013–
 231 2019 with WS decreasing from 2.2 m/s in 2013 to 1.4 m/s in 2019 (Fig. S7) and stable RH (Fig. S8).
 232 Similarly, summer CM reductions in 2013–2019 corresponded with WS declines. These patterns
 233 suggest spring-summer CM improvements resulted from the synergistic effects of meteorological
 234 changes and dust control policies. Conversely, autumn-winter seasons showed limited CM reductions
 235 despite comparable WS decreases in 2013–2019, highlighting the need for enhanced dust emission
 236 controls in Zhengzhou during these seasons. As for the individual crustal elements in Fig. S9, Ca
 237 exhibited the highest average annual decline rate of 33% during 2013–2019, followed by Al. Si showed
 238 a less pronounced decline, attributed to its association with soil dust, where control measures for
 239 exposed soil are lacking (Zhang et al., 2020). In addition, the Ca^{2+} concentration as depicted in Fig. 2c
 240 decreased from $3.2 \pm 2.1 \mu\text{g}/\text{m}^3$ in 2013 to $2.2 \pm 1.1 \mu\text{g}/\text{m}^3$ in 2019, with an approximate annual average
 241 decline rate of $0.32 \mu\text{g}/(\text{m}^3 \cdot \text{year})$ from LS slope [$4.14\text{E}-03 \mu\text{g}/(\text{m}^3 \cdot \text{year})$ from Sen's slope] in Table
 242 S6, further demonstrating the decline in dust source. It was worth noting that the proportions of CM,

243 Ca, Al, Fe, Si, and Ca^{2+} in $\text{PM}_{2.5}$ have shown consecutive annual increases from 2013 to 2019, with
244 CM proportion increasing from 8% in 2013 to 14% in 2019, indicating that CM reduction lagged
245 behind $\text{PM}_{2.5}$ reduction efforts in Zhengzhou during this period. Additionally, both concentration and
246 proportion of Ca^{2+} in 2022 ($2.2 \pm 1.1 \mu\text{g}/\text{m}^3$ and 5%) were higher than in other cities of China, such as
247 Beijing ($1.0 \mu\text{g}/\text{m}^3$ and 2.8%), Tianjin ($0.5 \mu\text{g}/\text{m}^3$ and 1.4%), and Xiamen ($0.48 \mu\text{g}/\text{m}^3$ and 1.5%) (Shi
248 et al., 2017; Xu et al., 2025; Zhang et al., 2021). These results indicate that CM remained an important
249 component of $\text{PM}_{2.5}$ in Zhengzhou City.

250 During 2019–2022, both CM and Ca^{2+} concentrations exhibited significant rebounds, with annual
251 growth rates of 0.24 and $0.4 \mu\text{g}/(\text{m}^3 \cdot \text{year})$ from LS slope [$5.80\text{E}-03$ and $5.42\text{E}-03 \mu\text{g}/(\text{m}^3 \cdot \text{year})$ from
252 Sen's slope], respectively, and their proportions increased from 14% and 2% in 2019 to 22% and 5%
253 in 2022. CM concentrations rebounded in all seasons, particularly in winter (Fig. S6). Changes in
254 meteorological conditions may be a significant factor contributing to these concentration rebounds,
255 accompanied by the average WS increased by 0.14 m/s and RH decreased by 7% from 2020 to 2022
256 (Fig. S5, S7, and S8), facilitating dust resuspension. Furthermore, the lack of more effective dust
257 control measures, as indicated by the absence of significant changes in the dust control policies from
258 the Air Pollution Prevention and Control Action Plan and Three-Year Action Plan, may be another
259 important factor contributing to the rebound of dust.

260 3.3 Sources of CM

261 Elemental ratios were employed to characterize the sources of CM, with the Ca/Al ratio widely
262 recognized as a reliable indicator of sandy origin (Zhang et al., 2017). In addition, significant variations

263 in Ca/Si ratios (Table S7) were observed among different dust sources (Road, Construction, Piles, Soil).
264 Fig. 3a illustrates the trend in Ca/Si ratios from 2011 to 2022. After 2013, Ca/Si ratios showed a
265 declining trend annually, with the average ratio decreasing from a peak of 1.6 in 2016 to a lowest of
266 0.4 in 2022. Compared with Ca/Si ratios from different types of dust sources, the effect of road and
267 construction dust on CM has gradually decreased. This may be attributed to the implementation of dust
268 control measures such as enclosure, shielding, and dust suppression at construction and demolition
269 sites, as well as dust control on ground surfaces and roads (Table S5). During 2019–2022, the average
270 Ca/Si ratio remained below 1, with a mean of 0.4 in 2022, indicating that soil dust predominantly
271 contributed to CM. Currently, measures for controlling soil-suspended dust are limited, primarily
272 relying on long-term strategies such as afforestation and increasing urban green coverage, thus
273 requiring a longer process and sustained investment.

274 Sand dust transport serves as a significant source of CM in the North China Plain (Zhang et al.,
275 2024). The Ca/Al ratio from 2016 to 2022 (Fig. 3b) shows minimal variation, with annual averages
276 ranging between 1.5 and 2.5, indicating no significant changes in the source regions of sand. The
277 transport trajectories (Fig. 3c and 3d) reveal that a marked decline in the contribution of long-distance
278 sand dust transport originating from Inner Mongolia (via Shaanxi and Shanxi provinces) from 13.9%
279 during 2013–2018 to 7.2% in 2019–2022. In contrast, local transport within Henan province and short-
280 distance transport from Shandong province exhibited contrasting increases. These findings suggest
281 that the rebound in CM concentrations during 2019–2022 in Zhengzhou might be responsible for the

282 resuspension of surrounding soil dust.

283 **3.4 Long-term trend of particle pH**

284 Are shown in Fig. 4 and Table S6, pH values showed a clearly increasing trend after 2014. From
285 2013 to 2019, the annual pH increased by 0.11 units from the LS slope [$9.15\text{E-}04$ units from Sen's
286 slope], reaching a maximum median value of 4.45 (Mean: 4.35) in 2018. Note that the annual average
287 growth rate of pH values increased to 0.21 units from LS slope [$2.93\text{E-}03$ units from Sen's slope] from
288 2019 to 2022, with a maximum median value of 4.42 (Mean: 4.51) in 2022. Seasonally, pH values
289 showed increasing trends in spring, summer, and autumn, and notably increased in winter from 2020
290 to 2022 (Fig. S10). The increasing trend in pH values observed in this study is similar to the findings
291 in Beijing (Song et al., 2019; Xie et al., 2020), presumably attributable to the comparable chemical
292 composition trends and meteorological conditions (Liu et al., 2017; Wang et al., 2020; Xu et al., 2015).
293 In contrast, Shanghai and Hong Kong display divergent trends (Nah et al., 2023; Zhou et al., 2022).
294 This disparity might be ascribed to the stronger buffering effect exerted by NH_3 and dust in Zhengzhou
295 than marine aerosols (Na^+/Cl^-) in these coastal cities (Shi et al., 2017; Liu et al., 2019). Moreover,
296 these coastal cities' warm climates amplify pH declines. Elevated temperatures reduce ALWC through
297 moisture evaporation, concentrating H^+ and directly lowering pH. Concurrently, heat-enhanced NH_3
298 volatilization from particulate NH_4^+ weakened acid neutralization (Zhou et al., 2022; Nah et al., 2023).

299 Sensitivity analyses were conducted to explore the dominant factors driving the elevated particle
300 pH in Zhengzhou by giving a range for one parameter (i.e., TNH_x) and average values for other
301 parameters (i.e., SO_4^{2-} , NO_3^- , Na^+ , Cl^- , Ca^{2+} , K^+ , Mg^{2+} , RH, and T) input into the ISORROPIA-II

302 model. Are shown in Fig. S11, particle pH increases with the cation concentrations (e.g., TNH_x , K^+ ,
303 Ca^{2+} , Mg^{2+} , and Na^+) and decreases with anion concentrations (e.g., SO_4^{2-} and NO_3^-). Additionally,
304 RH does not significantly affect pH, whereas an increase in T leads to a noticeable decrease in particle
305 pH.

306 Based on the sensitivity analysis curves, the pH values corresponding to a variable in different
307 years were calculated according to the average values of this variable in different years (Table S8).
308 The difference in pH values of this variable between two adjacent years was defined as ΔpH which is
309 illustrated in Fig. 5. According to Equation (2), in addition to H^+ concentration, particle pH is primarily
310 influenced by the dilution effect of ALWC. Moreover, ALWC affects the gas-particle partitioning of
311 semi-volatile compounds, thereby influencing particle acidity (Zuend et al., 2010; Zuend and Seinfeld,
312 2012). As shown in Fig.5 and Table S8, only in 2015, 2019, and 2020 did the increases in ALWC
313 concentration ($17.6 \mu\text{g}/\text{m}^3$, $4.1 \mu\text{g}/\text{m}^3$, and $11.6 \mu\text{g}/\text{m}^3$, respectively) lead to pH increases of 0.22, 0.06,
314 and 0.14 units. This clearly cannot fully explain the significant pH increase in Zhengzhou since 2013.
315 Notably, since 2013, H^+ concentration has shown a decreasing trend. Particularly, H^+ concentrations
316 decreased by 7.6×10^{-6} , 11.2×10^{-6} , and $7.2 \times 10^{-6} \text{ mol/L}$ in 2013, 2015, and 2017, respectively,
317 leading to pH increases of 0.21, 0.36, and 0.42 units. After 2019, a continuous decline in H^+
318 concentration was observed for three consecutive years, resulting in pH increases of 0.21, 0.13, and
319 0.2 units in 2020, 2021, and 2022, respectively. These findings indicate that the increase in pH from
320 2019 to 2022 in Zhengzhou was primarily driven by the reduction in H^+ concentration.

321 The concentration of H^+ in the aerosol liquid phase is influenced by both chemical composition
322 and meteorological conditions. To further understand the factors affecting ΔpH , we analyzed the

323 variations in PM_{2.5} chemical components and meteorological parameters. Results indicate that the
324 decline in SO₄²⁻ from 2013 to 2018 was the primary cause of the increase in particle pH, as it decreased
325 H⁺ and ALWC concentrations (Fig. S12) in aerosol (Ding et al., 2019; Zhang et al., 2021). The average
326 SO₄²⁻ concentration decreased by 14.6 and 5.3 µg/m³, resulting in a pH increase of 0.43 and 0.35 units
327 from 2013 to 2014 and 2016 to 2017, respectively, which was comparable to an increased rate of 0.3
328 units in East Asia due to SO₂ emission controls since 2016 (Karydis et al., 2021). As another acidic
329 ion, the decrease in nitrate concentration did not significantly contribute to the pH increases, consistent
330 with findings from Ding et al. (2019) and Zhang et al. (2021). This is primarily because NO₃⁻ declined
331 more slowly compared to sulfate ions and exceeded sulfate concentrations after 2016, under which
332 conditions that nitrate-rich particles can absorb twice the amount of water that sulfate-rich particles,
333 leading to an increase in ALWC concentration and inhibiting pH decline (Lin et al., 2020; Xie et al.,
334 2020). On the other hand, increases in particle pH in 2015 and 2018 were notably influenced by
335 changes in TNH_x with concentrations increased by 5.5 and 1.3 µg/m³, respectively. Increased TNH_x
336 concentrations could react with SO₄²⁻ or NO₃⁻ and consume a substantial amount of H⁺, thereby raising
337 particulate matter pH values (Seinfeld et al., 1998; Zhang et al., 2021). Substantial decreases in T in
338 2015 (4.2°C), 2017 (4.9°C), and 2018 (2.8°C), favoring NH₃ partitioning into the particle phase and
339 reducing H⁺ concentrations, drove increases in particle pH (Tao and Murphy, 2019).

340 During the period from 2020 to 2022, the influence of SO₄²⁻ on particle pH gradually decreased,
341 with a decrease in concentration from 0.3 to 2.3 µg/m³ (Table S8) only bringing about a pH decrease
342 of 0.03 to 0.14 (Fig. 5). Moreover, a rebound in SO₄²⁻ concentration to 7.9 ± 4.5 µg/m³ in 2022 even
343 resulted in a decrease of 0.11 units in pH instead. On the other hand, TNH_x began to show a slight

annual decline (0.9 to $2.2 \mu\text{g}/\text{m}^3$), resulting in a significant decrease in pH (0.21 – 0.35). Consequently, the increase in pH values was closely related to the rise in Ca^{2+} concentration. Ca^{2+} is less volatile and competes preferentially with NH_3 to neutralize anions such as SO_4^{2-} to form insoluble CaSO_4 , which precipitates from the aerosol aqueous phase (Ding et al., 2019; Karydis et al., 2021), thereby reducing H^+ concentrations (Fig. S12) and subsequently lowering particle acidity. Specifically, increases of 0.7 and $0.5 \mu\text{g}/\text{m}^3$ in Ca^{2+} concentrations led to pH increases of 0.13 and 0.09 units in 2020 and 2022, respectively, making Ca^{2+} a primary controlling factor for pH elevation.

4 Conclusions

The annual average $\text{PM}_{2.5}$ concentration in Zhengzhou decreased from $212.4 \pm 101.5 \mu\text{g}/\text{m}^3$ in 2013 to $59.5 \pm 41.2 \mu\text{g}/\text{m}^3$ in 2022, with the largest reduction in SO_4^{2-} . As for CM, their concentrations notably decreased from 2013 to 2019, because of effective dust control measures, as well as decreased wind speed and increased relative humidity. However, the proportions of CM in $\text{PM}_{2.5}$ have shown consecutive annual increases. In addition, CM concentrations and their proportions increased significantly during 2019–2022, which might be responsible for the resuspension of surrounding soil dust. Correspondingly, the annual pH increased by 0.11 units from 2013 to 2019 mainly due to the decline in SO_4^{2-} , increased TNH_x , or decreased temperature. During the period from 2020 to 2022, the annual average growth rate of pH values increased to 0.21 units from 2019 to 2022, which was determined by the rise in Ca^{2+} concentration.

5 Implication

Control measures implemented by the Chinese government have proven effective in reducing dust, but this study reveals that the crustal materials in $PM_{2.5}$ rebounded after 2019. This phenomenon is not unique to Zhengzhou, as major cities in the North China Plain have also experienced a pronounced upward trend in coarse particles after 2019 (Fig. S13). Thus, crustal materials persist as a substantial constituent of atmospheric aerosols in North China, sustaining elevated particle pH levels. Extensive research has established that heightened particle pH inhibits nitrate reduction in aerosols (Ding et al., 2019; Lin et al., 2020; Wen et al., 2018), particularly significant given nitrate's predominant role in haze formation within this region. Notably, while moderately acidic aerosols demonstrate reduced health impacts, particles with $pH < 3$ exhibit substantially greater health risks (Shi et al., 2019). Consequently, future environmental management strategies must prioritize real-time assessment of regulatory impacts on particle acidity. This necessitates an integrated approach that simultaneously addresses acidic precursors, alkaline precursors, and crustal material contributions to atmospheric acid chemistry.

Data availability

All the data presented in this article can be accessed through <https://doi.org/10.5281/zenodo.14032007> (Zhang, 2024).

379 **Supporting Information**

380 Additional data, figures, and tables, some of which are referenced directly within the manuscript,
381 and detailed descriptions of field measurements and samples.

382 **Author contributions**

383 S.W. designed this study. H.Z. and Z.D. analyzed the data and prepared the manuscript with the
384 contributions of all coauthors. X.L. conducted measurements. R.Z. provided funding acquisition. All
385 authors have read and agreed to the published version of the manuscript.

386 **Competing interests**

387 The authors declare that they have no conflict of interest.

388 **Acknowledgment**

389 This work was supported by the National Key R&D Program of China (No. 2024YFC3713701),
390 the China Postdoctoral Science Foundation (2023 M733220), the Zhengzhou PM_{2.5} and O₃
391 Collaborative Control and Monitoring Project (20220347 A), and the National Key R&D Program of
392 China (No. 2017YFC0212400).

Funding Sources

This work was supported by the National Key R&D Program of China (No. 2024YFC3713701), the China Postdoctoral Science Foundation (2023 M733220), the Zhengzhou PM_{2.5} and O₃ Collaborative Control and Monitoring Project (20220347 A), and the National Key R&D Program of China (No. 2017YFC0212400).

References

- Battaglia, M. A.; Douglas, S.; Hennigan, C.: Effect of the urban heat island on aerosol pH, *Environ. Sci. Technol.*, 51, 13095–13103, <https://doi.org/10.1021/acs.est.7b02786>, 2017.
- Chang, R. Y. W.; Slowik, J. G.; Shantz, N. C.; Vlasenko, A.; Liggio, J.; Sjostedt, S. J.; Leaitch, W. R.; Abbatt, J. P. D. The hygroscopicity parameter (κ) of ambient organic aerosol at a field site subject to biogenic and anthropogenic influences: relationship to degree of aerosol oxidation. *Atmos. Chem. Phys.*, 10, 5047–5064, <https://doi.org/10.5194/acp-10-5047-2010>, 2010.
- Ding, J., Zhao, P., Su, J., Dong, Q., Du, X., and Zhang, Y.: Aerosol pH and its driving factors in Beijing, *Atmos. Chem. Phys.*, 19, 7939–7954, <https://doi.org/10.5194/acp-19-7939-2019>, 2019.
- Dong, J., Li, B., Li, Y., Zhou, R., Gan, C., Zhao, Y., Liu, R., Yang, Y., Wang, T., and Liao, H.: Atmospheric ammonia in China: Long-term spatiotemporal variation, urban-rural gradient, and influencing factors, *Sci. Total Environ.*, 883, 163733, <https://doi.org/10.1016/j.scitotenv.2023.163733>, 2023.
- Fountoukis, C and Nenes, A.: ISORROPIA II: a computationally efficient thermodynamic equilibrium model for K⁺ - Ca²⁺ - Mg²⁺ - NH₄⁺ - Na⁺ - SO₄²⁻ - NO₃⁻ - Cl⁻ - H₂O aerosols, *Atmos. Chem. Phys.*, 7, 4639–4659, <https://doi.org/10.5194/acp-7-4639-2007>, 2007.
- Guo, H., Sullivan, A. P., Campuzano-Jost, P., Schroder, J. C., Lopez-Hilfiker, F. D., Dibb, J. E., Jimenez, J. L., Thornton, J. A., Brown, S. S., Nenes, A., and Weber, R. J.: Fine particle pH and the

partitioning of nitric acid during winter in the northeastern United States, *J. Geophys. Res. Atmos.*, 121, 10,355–310,376, <https://doi.org/10.1002/2016JD025311>, 2016.

Guo, H., Xu, L., Bougiatioti, A., Cerully, K. M., Capps, S. L., Hite Jr, J. R., Carlton, A. G., Lee, S. H., Bergin, M. H., Ng, N. L., Nenes, A., and Weber, R. J.: Fine-particle water and pH in the southeastern United States, *Atmos. Chem. Phys.*, 15, 5211–5228, <https://doi.org/10.5194/acp-15-5211-2015>, 2015.

Heald, C.; Collett, J. J.; Lee, T.; Benedict, K.; Schwandner, F.; Li, Y.; Clarisse, L.; Hurtmans, D. R.; Van, D. M.; Clerbaux, C.; Coheur, P. F., Philip, S.; Martin, R. V.; Pye, T.: Atmospheric ammonia and particulate inorganic nitrogen over the United States, *Atmos. Chem. Phys.*, 12, 10295–10312, <https://doi.org/10.5194/acp-12-10295-2012>, 2012.

Huang, X., Song, Y., Li, M., Li, J., Huo, Q., Cai, X., Zhu, T., Hu, M., and Zhang, H.: A high-resolution ammonia emission inventory in China, *Global. Biogeochem. Cy.*, 26, GB1030, <https://doi.org/10.1029/2011GB004161>, 2012.

Jiang, N.; Duan, S.; Yu, X.; Zhang, R.; Wang, K. Comparative major components and health risks of toxic elements and polycyclic aromatic hydrocarbons of PM_{2.5} in winter and summer in Zhengzhou: Based on three-year data. *Atmos. Res.*, 213, 173–184, <https://doi.org/10.1016/j.atmosres.2018.06.008>, 2018.

Karydis, V. A., Tsimpidi, A. P., Pozzer, A., and Lelieveld, J.: How alkaline compounds control atmospheric aerosol particle acidity, *Atmos. Chem. Phys.*, 21, 14983–15001, <https://doi.org/10.5194/acp-21-14983-2021>, 2021.

Kim, Y., Park, O., Park, S. H., Kim, M. J., Kim, J.-J., Choi, J.-Y., Lee, D., Cho, S., and Shim, S.: PM_{2.5} pH estimation in Seoul during the KORUS-AQ campaign using different thermodynamic models, *Atmos. Environ.*, 268, 118787, <https://doi.org/10.1016/j.atmosenv.2021.118787>, 2022.

Lei, L., Zhou, W., Chen, C., He, Y., Li, Z., Sun, J., Tang, X., Fu, P., Wang, Z., and Sun, Y.: Long-term characterization of aerosol chemistry in cold season from 2013 to 2020 in Beijing, China, *Environ. Pollut.*, 268, 115952, <https://doi.org/10.1016/j.envpol.2020.115952>, 2021.

Li, C.; Hu, Y.; Chen, J.; Ma, Z.; Ye, X.; Yang, X.; Wang, L.; Wang, X.; Mellouki, A. Physiochemical

properties of carbonaceous aerosol from agricultural residue burning: Density, volatility, and hygroscopicity. *Atmos. Environ.*, 140, 94–105, <https://doi.org/10.1016/j.atmosenv.2016.05.052>, 2016.

Li, W., Xu, L., Liu, X., Zhang, J., Lin, Y., Yao, X., Gao, H., Zhang, D., Chen, J., Wang, W., Harrison, R. M., Zhang, X., Shao, L., Fu, P., Nenes, A., and Shi, Z.: Air pollution-aerosol interactions produce more bioavailable iron for ocean ecosystems, *Sci. Adv.*, 3, e1601749, <https://doi.org/10.1126/sciadv.1601749>, 2017.

Li, Y., Lei, L., Sun, J., Gao, Y., Wang, P., Wang, S., Zhang, Z., Du, A., Li, Z., Wang, Z., Kim, J. Y., Kim, H., Zhang, H., and Sun, Y.: Significant reductions in secondary aerosols after the Three-Year Action Plan in Beijing summer, *Environ. Sci. Technol.*, 57, 15945–15955, <https://doi.org/10.1021/acs.est.3c02417>, 2023.

Lin, Y., Zhang, Y., Fan, M., and Bao, M.: Heterogeneous formation of particulate nitrate under ammonium-rich regimes during the high-PM_{2.5} events in Nanjing, China, *Atmos. Chem. Phys.*, 20, 3999–4011, <https://doi.org/10.5194/acp-20-3999-2020>, 2020.

Liu, M.; Huang, X.; Song, Y.; Tang, J.; Cao, J.; Zhang, X.; Zhang, Q.; Wang, S.; Xu, T.; Kang, L.; Gai, X.; Zhang, H.; Yang, F.; Wang, H.; Yu, J.; Lau, A.; He, L.; Huang, X.; Duan, L.; Ding, A.; Xue, L.; Gao, J.; Liu, B.; Zhu, T. Ammonia emission control in China would mitigate haze pollution and nitrogen deposition, but worsen acid rain. *Proc. Natl. Acad. Sci.*, 116, 7760–7765, <https://doi.org/10.1073/pnas.1814880116>, 2019.

Liu, M., Song, Y., Zhou, T., Xu, Z., Yan, C., Zheng, M., Wu, Z., Hu, M., Wu, Y., and Zhu, T.: Fine particle pH during severe haze episodes in northern China, *Geophys. Res. Lett.*, 44, 5213–5221, <https://doi.org/10.1002/2017GL073210>, 2017.

Liu, Z., Gao, W., Yu, Y., Hu, B., Xin, J., Sun, Y., Wang, L., Wang, G., Bi, X., Zhang, G., Xu, H., Cong, Z., He, J., Xu, J., and Wang, Y.: Characteristics of PM_{2.5} mass concentrations and chemical species in urban and background areas of China: emerging results from the CARE-China network, *Atmos. Chem. Phys.*, 18, 8849–8871, <https://doi.org/10.5194/acp-18-8849-2018>, 2018.

Mao, I., Lin, C., Lin, C., Chen, Y., Sung, F., and Chen, M.: Exposure of acid aerosol for

470 schoolchildren in metropolitan Taipei, *Atmos. Environ.*, 43, 5622–5629, [https://doi.org/10.](https://doi.org/10.1016/j.atmosenv.2009.07.054)
 471 [1016/j.atmosenv.2009.07.054](https://doi.org/10.1016/j.atmosenv.2009.07.054), 2009.

472 Masiol, M., Squizzato, S., Formenton, G., Khan, M. B., Hopke, P. K., Nenes, A., Pandis, S. N., Tositti,
 473 L., Benetello, F., Visin, F., and Pavoni, B.: Hybrid multiple-site mass closure and source
 474 apportionment of PM_{2.5} and aerosol acidity at major cities in the Po Valley, *Sci. Total Environ.*,
 475 704, 135287, <https://doi.org/10.1016/j.scitotenv.2019.135287>, 2020.

476 MEP (Ministry of Environment Protection), 2023. [https://www.mee.gov.cn/ywdt/hjywnews/2024](https://www.mee.gov.cn/ywdt/hjywnews/202406/t20240605_1075031.shtml)
 477 [06/t20240605_1075031.shtml](https://www.mee.gov.cn/ywdt/hjywnews/202406/t20240605_1075031.shtml), Accessed date:5 June 2024.

478 Nah, T., Lam, Y. H., Yang, J., and Yang, L.: Long-term trends and sensitivities of PM_{2.5} pH and aerosol
 479 liquid water to chemical composition changes and meteorological parameters in Hong Kong,
 480 South China: Insights from 10-year records from three urban sites, *Atmos. Environ.*, 302,
 481 <https://doi.org/10.1016/j.atmosenv.2023.119725>, 2023.

482 Nenes, A., Pandis, S. N., Kanakidou, M., Russell, A. G., Song, S., Vasilakos, P., and Weber, R. J.:
 483 Aerosol acidity and liquid water content regulate the dry deposition of inorganic reactive nitrogen,
 484 *Atmos. Chem. Phys.*, 21, 6023–6033, <https://doi.org/10.5194/acp-21-6023-2021>, 2021.

485 Pinder, R., Adams, P., and Pandis, S.: Ammonia emission controls as a cost-effective strategy for
 486 reducing atmospheric particulate matter in the eastern United States, *Environ. Sci. Technol.*, 41,
 487 380–386, <https://doi.org/10.1021/es060379a>, 2007.

488 Pinder, R., Gilliland, A., and Dennis, R.: Environmental impact of atmospheric NH₃ emissions under
 489 present and future conditions in the eastern United States, *Geophys. Res. Lett.*, 35, 28,
 490 <https://doi.org/10.1029/2008gl033732>, 2008.

491 Pye, H. O. T.; Nenes, A.; Alexander, B.; Ault, A. P.; Barth, M. C.; Clegg, S. L.; Collett Jr, J. L.; Fahey,
 492 K. M.; Hennigan, C. J.; Herrmann, H.; Kanakidou, m.; Kelly, J. T.; Ku, L.; McNeill, V. F.; Riemer,
 493 N.; Schaefer, T.; Shi, G.; Tilgner, A.; Walker, J.T.; Wang, T.; Weber, R.; Xing, J.; Zaveri, R. A.;
 494 Zuend, A. The acidity of atmospheric particles and clouds. *Atmos. Chem. Phys.*, 20, 4809–4888,
 495 <https://doi.org/10.5194/acp-20-4809-2020>, 2020.

496 Rengarajan, R., Sudheer, A. K., and Sarin, M. M.: Aerosol acidity and secondary organic aerosol

497 formation during wintertime over urban environment in western India, *Atmos. Environ.*, 45,
 498 1940–1945, <https://doi.org/10.1016/j.atmosenv.2011.01.026>, 2011.

499 Seinfeld, J. H., Pandis, S. N., and Noone, K. J.: Atmospheric chemistry and physics: From air pollution
 500 to climate change, *Phys. Today.*, 51, 88–90, <https://doi.org/10.1063/1.882420>, 1998.

501 Sharma, B., Jia, S., Polana, A. J., Ahmed, M. S., Haque, R. R., Singh, S., Mao, J., and Sarkar, S.:
 502 Seasonal variations in aerosol acidity and its driving factors in the eastern Indo-Gangetic Plain:
 503 A quantitative analysis, *Chemosphere.*, 305, 135490,
 504 <https://doi.org/10.1016/j.chemosphere.2022.135490>, 2022.

505 Shi, G., Xu, J., Peng, X., Xiao, Z., Chen, K., Tian, Y., Guan, X., Feng, Y., Yu, H., Nenes, A., and Russell,
 506 A. G.: pH of aerosols in a polluted atmosphere: source contributions to highly acidic aerosol,
 507 *Environ. Sci. Technol.*, 51, 4289–4296, <https://doi.org/10.1021/acs.est.6b05736>, 2017.

508 Shi, X., Nenes, A., Xiao, Z., Song, S., Yu, H., Shi, G., Zhao, Q., Chen, K., Feng, Y., and Russell, A.
 509 G.: High-resolution data sets unravel the effects of sources and meteorological conditions on
 510 nitrate and its gas-particle partitioning, *Environ. Sci. Technol.*, 53, 3048–3057,
 511 <https://doi.org/10.1021/acs.est.8b06524>, 2019.

512 Song, S., Nenes, A., Gao, M., Zhang, Y., Liu, P., Shao, J., Ye, D., Xu, W., Lei, L., Sun, Y., Liu, B.,
 513 Wang, S., and McElroy, M. B.: Thermodynamic modeling suggests declines in water uptake and
 514 acidity of inorganic aerosols in Beijing winter haze events during 2014/2015–2018/2019, *Environ.*
 515 *Sci. Technol. Lett.*, 6, 752–760, <https://doi.org/10.1021/acs.estlett.9b00621>, 2019.

516 Su, H., Cheng, Y., and Pöschl, U.: New Multiphase Chemical Processes Influencing Atmospheric
 517 Aerosols, Air Quality, and Climate in the Anthropocene, *Acc. Chem. Res.*, 53, 2034–2043,
 518 <https://doi.org/10.1021/acs.accounts.0c00246>, 2020.

519 Surratt, J. D., Chan, A. W. H., Eddingsaas, N. C., Chan, M., Loza, C. L., Kwan, A. J., Hersey, S. P.,
 520 Flagan, R. C., Wennberg, P. O., and Seinfeld, J. H.: Reactive intermediates revealed in
 521 secondary organic aerosol formation from isoprene, *Proc. Natl. Acad. Sci.*, 107, 6640–6645,
 522 <https://doi.org/10.1073/pnas.0911114107>, 2010.

523 Tao, Y. and Murphy, J. G.: The sensitivity of PM_{2.5} acidity to meteorological parameters and chemical

composition changes: 10-year records from six Canadian monitoring sites, *Atmos. Chem. Phys.*, 19, 9309–9320, <https://doi.org/10.5194/acp-19-9309-2019>, 2019.

Tian, Y.; Chen, G.; Wang, H.; Huang-Fu, Y.; Shi, G.; Han, B.; and Feng, Y.: Source regional contributions to PM_{2.5} in a megacity in China using an advanced source regional apportionment method. *Chemosphere.*, 147, 256–263, <https://doi.org/10.1016/j.chemosphere.2015.12.132>, 2016.

Tremper, A.; Font, A.; Priestman, M.; Hamad, S.; Chung, T.; Pribadi, A.; Brown, R.; Goddard, S.; Grassineau, N.; Petterson, K.; Kelly, F.; Green, D.: Field and laboratory evaluation of a high time resolution x-ray fluorescence instrument for determining the elemental composition of ambient aerosols, *Atmos. Meas. Tech.*, 11, 3541–3557, <https://doi.org/10.5194/amt-11-3541-2018>, 2018.

Wang, C., Yin, S., Bai, L., Zhang, X., Gu, X., Zhang, H., Lu, Q., and Zhang, R.: High-resolution ammonia emission inventories with comprehensive analysis and evaluation in Henan, China, 2006–2016, *Atmos. Environ.*, 193, 11–23, <https://doi.org/10.1016/j.atmosenv.2018.08.063>, 2018.

Wang, G., Chen, J., Xu, J., Yun, L., Zhang, M., Li, H., Qin, X., Deng, C., Zheng, H., Gui, H., Liu, J., and Huang, K.: Atmospheric processing at the Sea-Land interface over the South China Sea: Secondary aerosol formation, aerosol acidity, and role of sea salts, *J. Geophys. Res. Atmos.*, 127, <https://doi.org/10.1029/2021jd036255>, 2022.

Wang, J.; Gao, J.; Che, F.; Wang, Y.; Lin, P.; Zhang, Y.: Dramatic changes in aerosol composition during the 2016–2020 heating seasons in Beijing–Tianjin–Hebei region and its surrounding areas: The role of primary pollutants and secondary aerosol formation, *Sci. Total Environ.*, 849, 157621, <https://doi.org/10.1016/j.scitotenv.2022.157621>, 2022.

Wang, L., Du, H., Chen, J., Zhang, M., Huang, X., Tan, H., Kong, L., and Geng, F.: Consecutive transport of anthropogenic air masses and dust storm plume: Two case events at Shanghai, China, *Atmos. Res.*, 127, 22–33, <https://doi.org/10.1016/j.atmosres.2013.02.011>, 2013.

Wang, S., Yin, S., Zhang, R., Yang, L., Zhao, Q., Zhang, L., Yan, Q., Jiang, N., and Tang, X.: Insight into the formation of secondary inorganic aerosol based on high-time-resolution data during haze episodes and snowfall periods in Zhengzhou, China, *Sci. Total Environ.*, 660, 47–56, <https://doi.org/10.1016/j.scitotenv.2018.12.465>, 2019.

551 Wang, S.; Wang, L.; Li, Y.; Wang, C.; Wang, W.; Yin, S.; Zhang, R.; Effect of ammonia on fine-particle
 552 pH in agricultural regions of China: comparison between urban and rural sites, *Atmos. Chem.*
 553 *Phys.*, 20, 2719–2734, <https://doi.org/10.5194/acp-20-2719-2020>, 2020.

554 Wang, Y. Q., Zhang, X. Y., and Draxler, R. R.: TrajStat: GIS-based software that uses various trajectory
 555 statistical analysis methods to identify potential sources from long-term air pollution
 556 measurement data, *Environ. Model. Softw.*, 24, 938–939,
 557 <https://doi.org/10.1016/j.envsoft.2009.01.004>, 2009.

558 Wang, Z., Pan, X., Uno, I., Chen, X., Yamamoto, S., Zheng, H., Li, J., and Wang, Z.: Importance of
 559 mineral dust and anthropogenic pollutants mixing during a long-lasting high PM event over East
 560 Asia, *Environ. Pollut.*, 234, 368–378, <https://doi.org/10.1016/j.envpol.2017.11.068>, 2018.

561 Weber, R.; Guo, H.; Russell, A.; Nenes, A.: High aerosol acidity despite declining atmospheric sulfate
 562 concentrations over the past 15 years, *Nature Geoscience.*, 9, 282–285,
 563 <https://doi.org/10.1038/ngeo2665>, 2016.

564 Wei, Y.; Wang, S.; Jiang, N.; Zhang, R.; and Hao, Q. Comparative multi-model study of PM_{2.5} acidity
 565 trend changes in ammonia-rich regions in winter: Based on a new ammonia concentration
 566 assessment method, *J. Hazard.*, 458, 15, <https://doi.org/10.1016/10.1016/j.jhazmat.2023.131970>,
 567 2023.

568 Wen, L., Xue, L., Wang, X., Xu, C., Chen, T., Yang, L., Wang, T., Zhang, Q., and Wang, W.:
 569 Summertime fine particulate nitrate pollution in the North China Plain: increasing trends,
 570 formation mechanisms and implications for control policy, *Atmos. Chem. Phys.*, 18, 11261–
 571 11275, <https://doi.org/10.5194/acp-18-11261-2018>, 2018.

572 Wexler, A. S. and Seinfeld, J. H.: Second-generation inorganic aerosol model, *Atmos. Environ.*, Part
 573 A. General Topics, 25, 2731–2748, [https://doi.org/10.1016/0960-1686\(91\)90203-J](https://doi.org/10.1016/0960-1686(91)90203-J), 1991.

574 Xie, Y., Wang, G., Wang, X., Chen, J., Chen, Y., Tang, G., Wang, L., Ge, S., Xue, G., Wang, Y., and
 575 Gao, J.: Nitrate-dominated PM_{2.5} and elevation of particle pH observed in urban Beijing during
 576 the winter of 2017, *Atmos. Chem. Phys.*, 20, 5019–5033, [https://doi.org/10.5194/acp-20-5019-](https://doi.org/10.5194/acp-20-5019-2020)
 577 [2020](https://doi.org/10.5194/acp-20-5019-2020), 2020.

578 Xu, K., Yin, L., Chen, Q., Liao, D., Ji, X., Zhang, K., Wu, Y., Xu, L., Li, M., Fan, X., Zhang, F., Huang,
 579 Z., Chen, J., and Hong, Y.: Quantitative analysis of influencing factors to aerosol pH and its
 580 responses to PM_{2.5} and O₃ pollution in a coastal city, *J. Environ. Sci.*, 151, 284–297,
 581 <https://doi.org/10.1016/j.jes.2024.03.044>, 2025.

582 Yu, F., Yan, Q., Jiang, N., Su, F., Zhang, L., Yin, S., Li, Y., Zhang, R., and Chen, L.: Tracking pollutant
 583 characteristics during haze events at background site Zhongmu, Henan Province, China, *Atmos.*
 584 *Pollut. Res.*, 8, 64–73, <https://doi.org/10.1016/j.apr.2016.07.005>, 2017.

585 Zhai, S.; Jacob, DJ.; Wang, X.; Shen, L.; Li, K.; Zhang, Y.; Gui, K.; Zhao, T.; Liao, H. Fine particulate
 586 matter (PM_{2.5}) trends in China, 2013–2018: separating contributions from anthropogenic
 587 emissions and meteorology, *Atmos. Chem. Phys.*, 19, 11031–11041, [https://doi.org/10.5194/acp-](https://doi.org/10.5194/acp-19-11031-2019)
 588 [19-11031-2019](https://doi.org/10.5194/acp-19-11031-2019), 2019.

589 Zhang, B., Shen, H., Liu, P., Guo, H., Hu, Y., Chen, Y., Xie, S., Xi, Z., Skipper, T. N., and Russell, A.
 590 G.: Significant contrasts in aerosol acidity between China and the United States, *Atmos. Chem.*
 591 *Phys.*, 21, 8341–8356, <https://doi.org/10.5194/acp-21-8341-2021>, 2021.

592 Zhang, G., Ding, C., Jiang, X., Pan, G., Wei, X., and Sun, Y.: Chemical compositions and sources
 593 contribution of atmospheric particles at a typical steel industrial urban site, *Sci. Rep.*, 10, 7654,
 594 <https://doi.org/10.1038/s41598-020-64519-x>, 2020.

595 Zhang, Z., Dong, Z., Zhang, C., Qian, G., and Lei, C.: The geochemical characteristics of dust material
 596 and dust sources identification in northwestern China, *J. Geochem. Explor.*, 175, 148–155,
 597 <https://doi.org/10.1016/j.gexplo.2016.11.006>, 2017.

598 Zhang, Z., Kuang, Z., Yu, C., Wu, D., Shi, Q., Zhang, S., Wang, Z., and Liu, D.: Trans–boundary dust
 599 transport of dust storms in Northern China: A study utilizing ground–based lidar network and
 600 CALIPSO satellite, *Remote sens.*, 16, 1196, <https://doi.org/10.3390/rs16071196>, 2024.

601 Zheng, G., Su, H., and Cheng, Y.: Revisiting the key driving processes of the decadal trend of aerosol
 602 acidity in the U.S, *Acs. Environ. Au.*, 2, 346–353, <https://doi.org/10.1021/acsenvironau.1c00055>,
 603 2022.

604 Zheng, G., Su, H., Wang, S., Andreae, M. O., Pöschl, U., and Cheng, Y.: Multiphase buffer theory

605 explains contrasts in atmospheric aerosol acidity, *Science.*, 369, 1374–1377,
 606 <https://doi.org/10.1126/science.aba3719>, 2020.

607 Zhou, M., Zheng, G., Wang, H., Qiao, L., Zhu, S., Huang, D., An, J., Lou, S., Tao, S., Wang, Q., Yan,
 608 R., Ma, Y., Chen, C., Cheng, Y., Su, H., and Huang, C.: Long-term trends and drivers of aerosol
 609 pH in eastern China, *Atmos. Chem. Phys.*, 22, 13833–13844, [https://doi.org/10.5194/acp-22-](https://doi.org/10.5194/acp-22-13833-2022)
 610 [13833-2022](https://doi.org/10.5194/acp-22-13833-2022), 2022.

611 Zhou, W., Gao, M., He, Y., Wang, Q., Xie, C., Xu, W., Zhao, J., Du, W., Qiu, Y., Lei, L., Fu, P., Wang,
 612 Z., Worsnop, D. R., Zhang, Q., and Sun, Y.: Response of aerosol chemistry to clean air action in
 613 Beijing, China: Insights from two-year ACSM measurements and model simulations, *Environ*
 614 *Pollut.*, 255, 113345, <https://doi.org/10.1016/j.envpol.2019.113345>, 2019.

615 Zuend, A. and Seinfeld, J. H.: Modeling the gas-particle partitioning of secondary organic aerosol: the
 616 importance of liquid-liquid phase separation, *Atmos. Chem. Phys.*, 12, 3857–3882,
 617 <https://doi.org/10.5194/acp-12-3857-2012>, 2012.

618 Zuend, A., Marcolli, C., Peter, T., and Seinfeld, J. H.: Computation of liquid-liquid equilibria and phase
 619 stabilities: implications for RH-dependent gas/particle partitioning of organic-inorganic aerosols,
 620 *Atmos. Chem. Phys.*, 10, 7795–7820, <https://doi.org/10.5194/acp-10-7795-2010>, 2010.

621

623

624

625

626

627

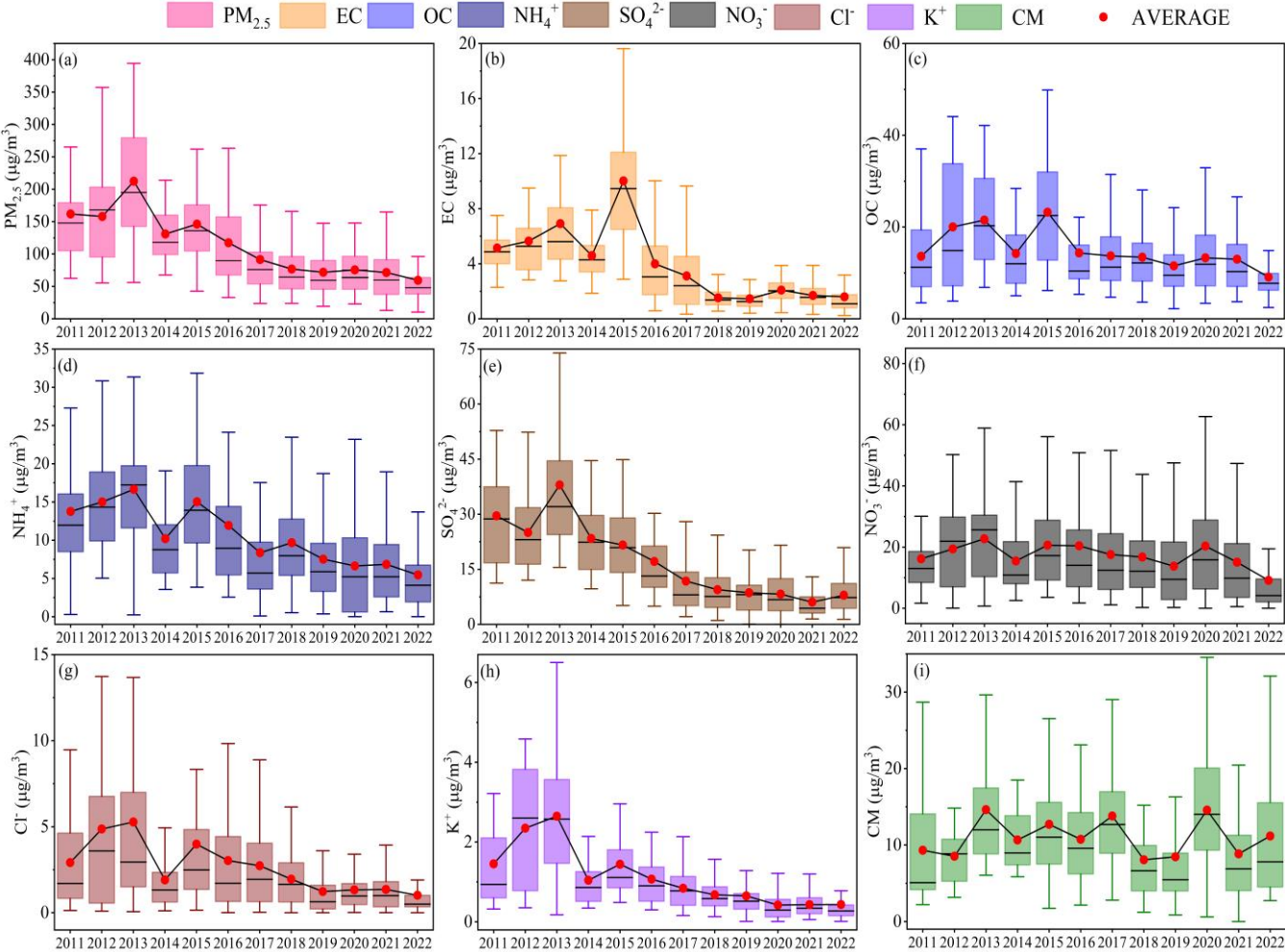
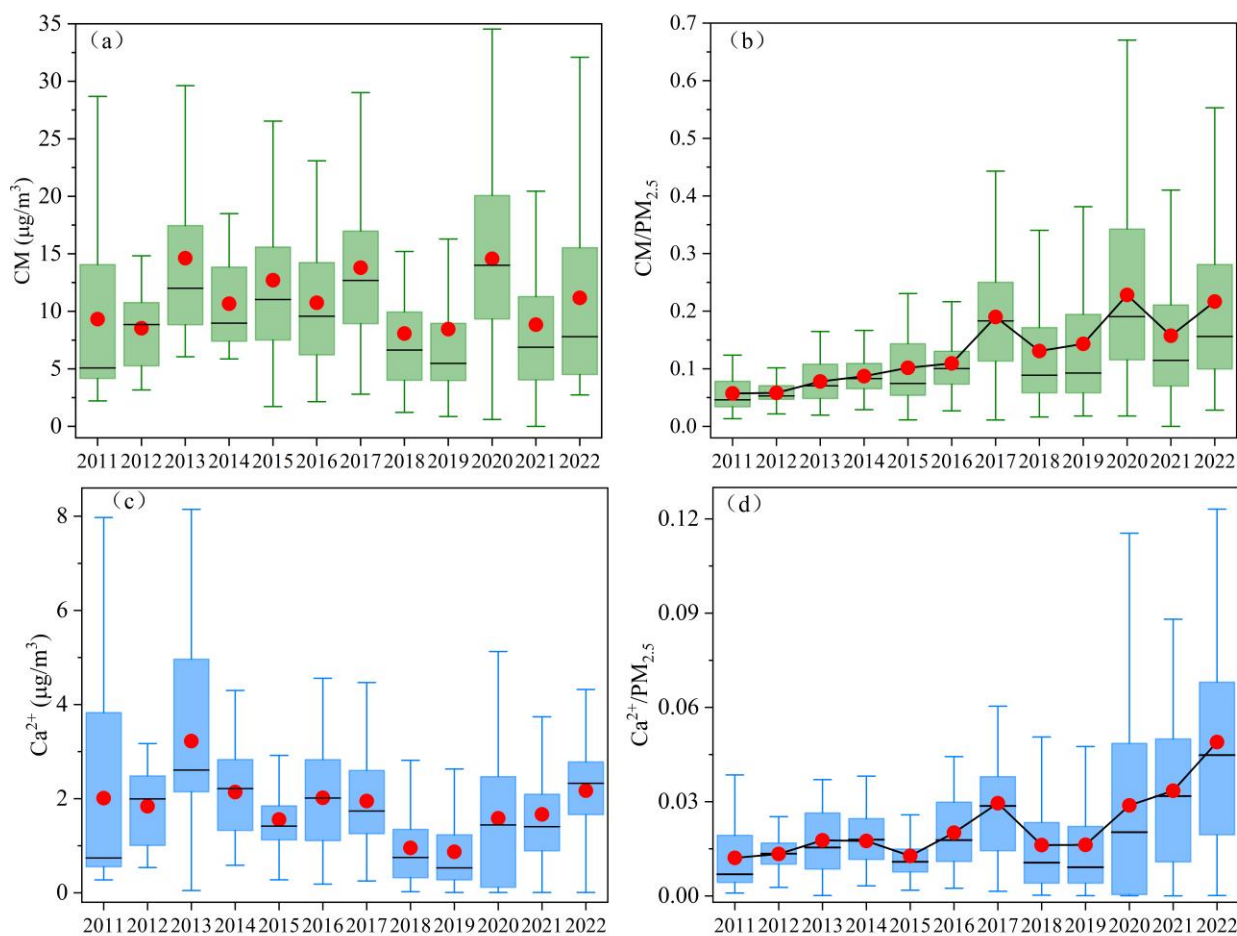


Figure 1. Long-term trends in the concentrations of $PM_{2.5}$ and its chemical components in from 2011 to 2022 in Zhengzhou. Box plots depict annual averages (red dots) and medians (black lines), the top, middle, and bottom lines represent the 75, 50, and 25 percentiles of statistical data, respectively, and the upper and lower whiskers represent the 90 and 10 percentiles of statistical data, respectively.



628

629 Figure 2. (a) and (c) Long-term trends in CM and Ca²⁺ concentrations in Zhengzhou from 2011 to
 630 2022, respectively. Box plots depict annual averages (red dots) and medians (black lines). (b) and (d)
 631 Long-term trends in the proportions of CM and Ca²⁺ in PM_{2.5}, respectively.

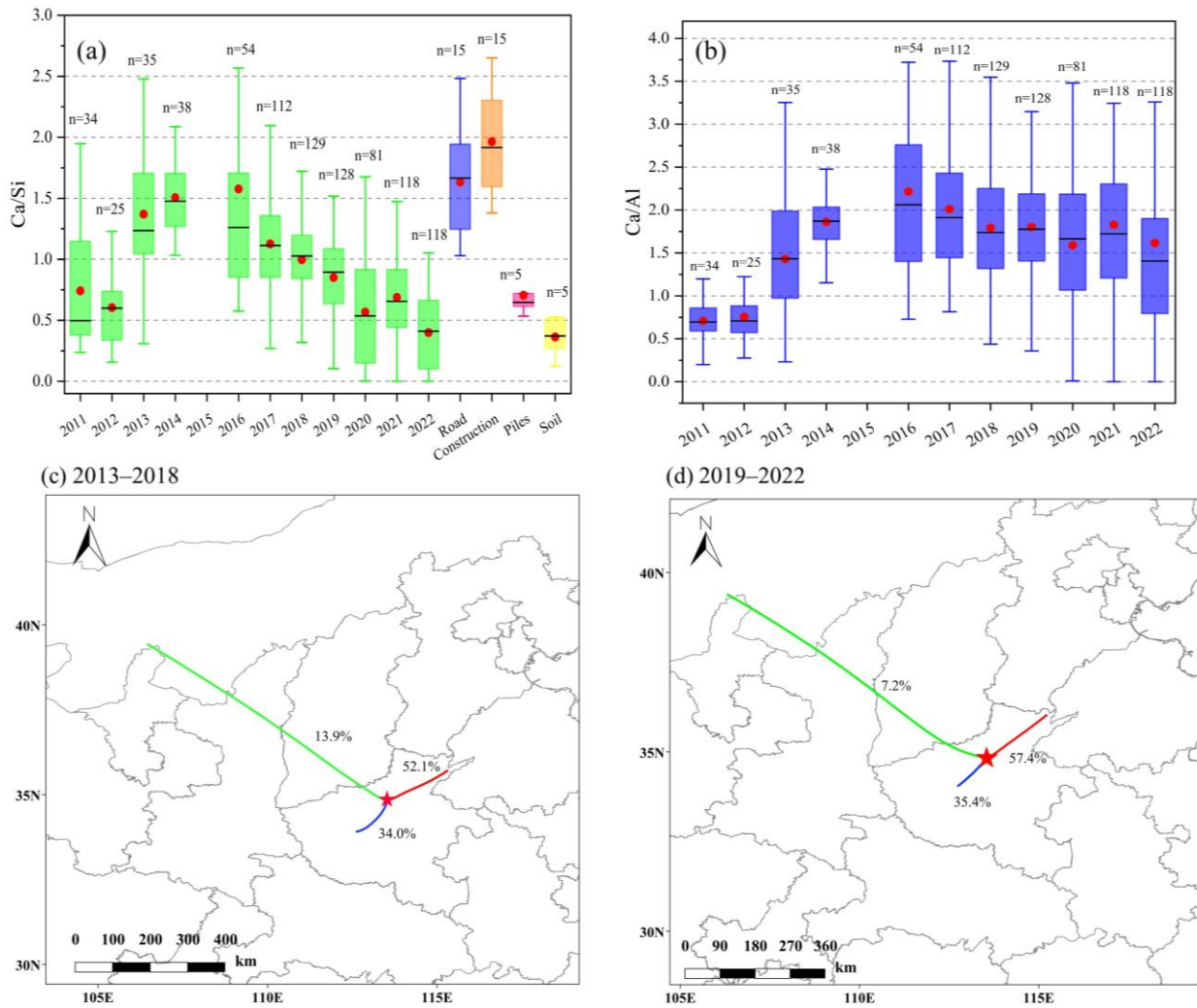
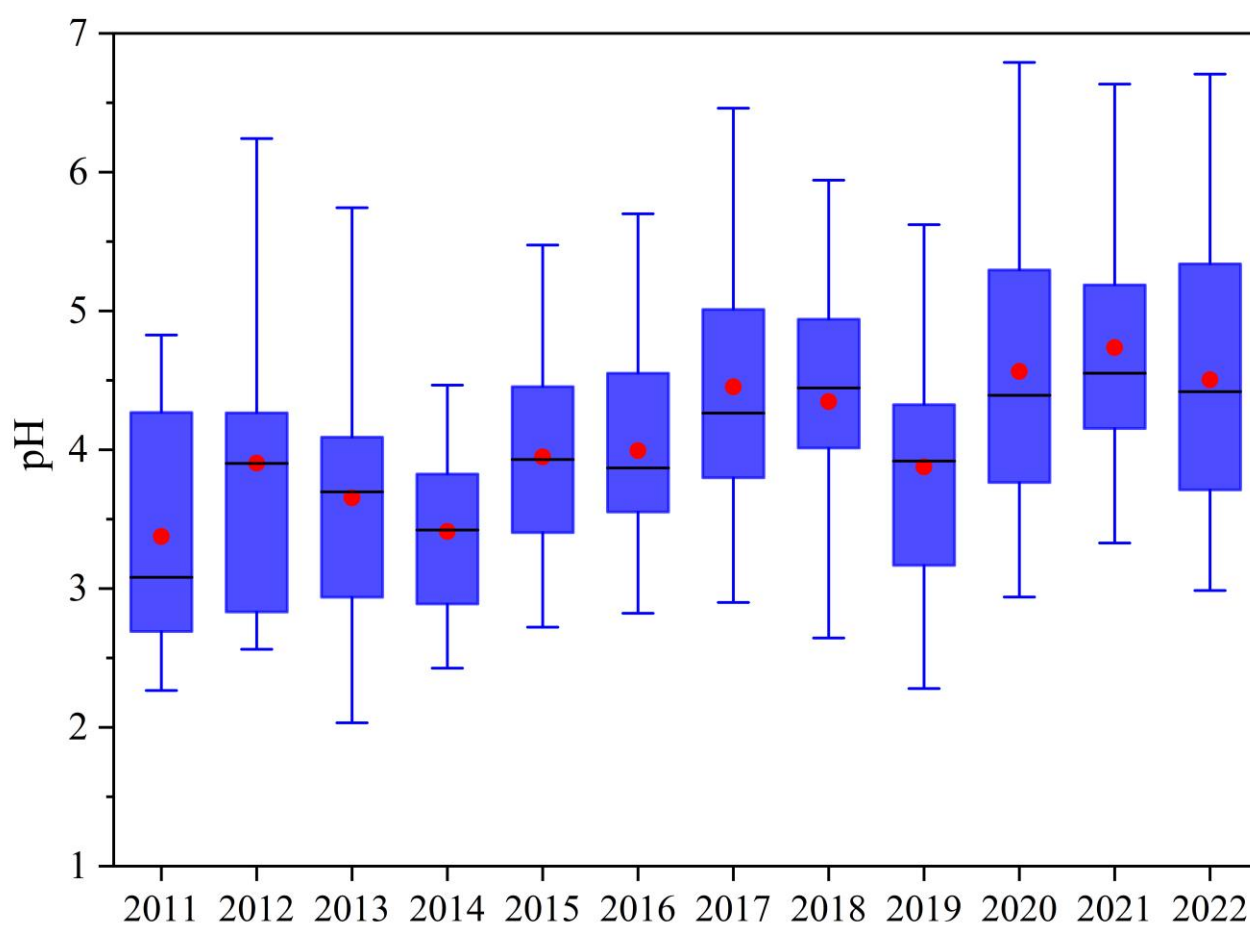


Figure 3. (a) The annual Ca/Si ratios in Zhengzhou from 2011 to 2022 compared with those in various dust sources (specific values and references in Table S7). The red dots and black lines in the box plots represent the annual averages and medians, respectively, with n indicating the sample size. (b) The Ca/Al ratios in Zhengzhou from 2011 to 2022. The red dots and black lines in the box plots represent the annual averages and medians, respectively, with n indicating the sample size. (c) and (d) The transport pathways of CM during 2013–2018 and 2019–2022, respectively.



639

640 Figure 4. The time series of particle pH in Zhengzhou from 2011 to 2022. In the boxplots, red dots
 641 and black lines represent the annual mean and median values, respectively.

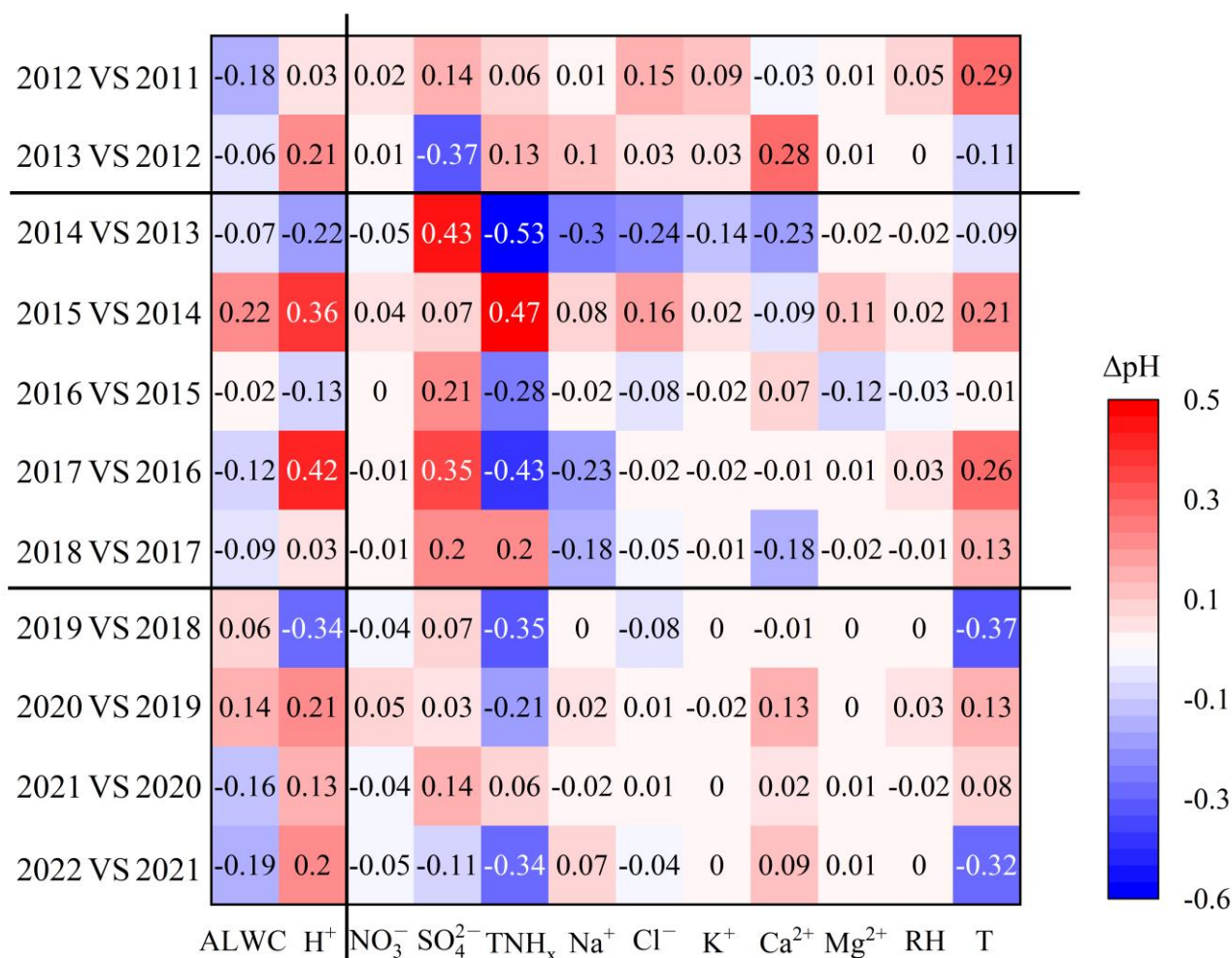


Figure 5. Contribution of each component to the changes in pH (ΔpH) between adjacent years. The difference between component concentrations and meteorological parameters between adjacent years is listed in Table S8.

646 **Table**

647 Table 1. Annual average concentrations of PM_{2.5} and its components from 2011 to 2022 in Zhengzhou,
648 China (µg/m³).

Years	PM _{2.5}	EC	OC	NO ₃ ⁻	SO ₄ ²⁻	NH ₄ ⁺	CM	Ca ²⁺
2011	161.9±81.4	5.1±2.1	13.6±8.6	16.2±11.2	29.6±14.3	13.8±8.3	9.3±7.3	2.0±2.2
2012	157.9±71.2	5.6±2.5	20.0±13.4	20.2±13.7	25.0±11.2	15.0±7.1	8.5±3.4	1.8±0.8
2013	212.4±101.5	6.9±3.8	21.5±10.4	22.7±13.2	38.0±19.9	17.1±6.9	14.6±8.3	3.2±2.1
2014	130.8±48.7	4.6±2.0	14.2±8.2	15.5±10.8	23.4±9.3	10.2±6.2	10.7±4.4	2.1±1.0
2015	146.1±61.0	10.0±4.7	23.2±11.6	20.6±14.5	21.6±9.8	15.7±7.5	12.7±6.8	1.6±0.7
2016	117.4±73.5	4.0±2.8	14.4±10.0	20.4±18.7	17.1±11.3	11.9±10.6	10.8±5.3	2.0±1.1
2017	91.5±61.1	3.1±2.5	13.7±7.5	17.6±15.9	11.8±11.6	8.4±7.9	13.8±6.5	2.0±1.0
2018	76.8±41.6	1.5±0.7	13.4±7.3	16.7±13.5	9.4±6.0	9.7±6.1	8.1±5.7	1.0±0.8
2019	68.4±34.8	1.5±0.8	11.5±6.8	13.8±13.9	8.6±6.4	7.5±6.1	8.5±7.8	0.9±0.9
2020	75.5±31.8	2.1±0.9	13.3±7.9	18.6±14.2	8.3±5.6	6.7±6.6	14.6±7.6	1.6±1.4
2021	71.5±45.9	1.7±0.9	13.0±8.0	15.1±15.1	6.1±4.5	6.8±6.0	8.9±7.0	1.7±1.2
2022	59.5±41.1	1.6±1.5	9.1±8.1	10.0±14.4	7.9±4.5	5.5±5.4	11.2±8.3	2.2±1.1

649

650